Available online at www.sciencedirect.com
ScienceDirect
Surface Science 600 (2006) 3780–3784
SURFACE SCIENCE
www.elsevier.com/locate/susc

Surface microstructure of the oxide protective layers grown on vanadium-free Ti alloys for use in biomedical applications

Alejandro Gutiérrez [a,*], Carmen Munuera [b], María Francisca López [b], José Antonio Jiménez [c], Carmen Morant [a], Thomas Matzelle [d], Norbert Kruse [d], Carmen Ocal [b]

[a] Departamento de Física Aplicada, Universidad Autónoma de Madrid, Cantoblanco, E-28049 Madrid, Spain
[b] Instituto de Ciencia de Materiales de Madrid, CSIC, Cantoblanco, E-28049 Madrid, Spain
[c] Centro Nacional de Investigaciones Metalúrgicas, CSIC, Avda. Gregorio del Amo 8, E-28040 Madrid, Spain
[d] Chimie-Physique des Matériaux, Université Libre de Bruxelles, La Plaine CP243, B-1050 Bruxelles, Belgium

Available online 17 April 2006

Abstract

In this work, we present a surface study by SFM (scanning force microscopy) of three new Ti alloys of composition (in wt%) Ti–7Nb–6Al, Ti–13Nb–13Zr and Ti–15Zr–4Nb, developed for biomedical applications. V was not included in these alloys since this element has been reported to be cytotoxic. The surface of these materials has been modified by a thermal treatment in air at 750 °C for different times. As a consequence of this treatment an oxide layer develops on the surface, resulting in both an improvement of the corrosion resistance and an increase of the roughness, which enhances the adhesion of the tissue cells to the implant. SFM has been used to characterize the surface structure and topography of the oxide layers grown on the three alloys. The surface roughness analysis obtained by SFM points to a correlation between the mean square roughness, the thickness of the oxide layer, and the α-phase/β-phase ratio in the base material.

Keywords: SFM; Oxidation; Biomaterials; Ti alloys

1. Introduction

Titanium and titanium alloys are extensively used as biomedical implant materials because their good mechanical properties are accompanied by an excellent biocompatibility [1,2]. Pure titanium and Ti alloys spontaneously develop a protective passive layer, few nanometers thick, when exposed to an oxygen-containing atmosphere. This layer confers a high biocompatibility, associated with a high corrosion resistance in aggressive biological environments. However, in osteoarticular implants, corrosion and wear processes produce metal ions release, which can be harmful for the organism. The most widely used Ti alloy for medical implants, Ti–6Al–4V, has V as one of its constituents. Since vanadium is known to be a cytotoxic element, alternative Ti–based alloys with other alloying elements are currently the subject of intensive study as new biomaterials [3–5]. Ti–6Al–4V belongs to the α–β family of Ti alloys, with a balance of alloying elements that results in a mixture of α and β phases at room temperature providing excellent mechanical properties to this alloy [6]. Whereas Al is an α-phase stabilizer, the high-temperature β-phase is stabilized, at room temperature, by certain alloying elements, such as Nb or V. Other elements, as Zr, are neutral with respect to phase stabilization. Thus, the use of alternative Ti alloys with the appropriate weight percentage of non-toxic elements would lead to a similar α–β phase ratio, and subsequently similar mechanical behaviour, to those of Ti–6Al–4V.

Surface modification of biomaterials is commonly applied to increase their corrosion and wear resistance. The resulting surface should be at least as biocompatible as

* Corresponding author. Fax: +34 91 497 39 69.
E-mail address: a.gutierrez@uam.es (A. Gutiérrez).

0039-6028/$ - see front matter © 2006 Published by Elsevier B.V.
doi:10.1016/j.susc.2006.01.082

the non-modified material. Furthermore, the technique used should be economically affordable to be a real alternative. In previous works, three Ti alloys without V, of composition (in wt%) Ti–7Nb–6Al, Ti–13Nb–13Zr and Ti–15Zr–4Nb, have been characterized as potential biomaterials [7,8]. These are α–β Ti alloys that are expected to resemble the good mechanical properties of Ti–6Al–4V. The chemical composition of Ti–7Nb–6Al and Ti–15Zr–4Nb alloys meets the requirements of reproducing the α-phase/β-phase volume ratio of the alloy to be replaced (i.e., Ti–6Al–4V), while keeping its good oxidation resistance. On the other hand, Ti–13Nb–13Zr, with a lower α-phase/β-phase ratio, has been included in the study for comparative purposes because it has been proposed as potential biomaterial [5], and because it has the same alloying elements as Ti–15Zr–4Nb, although with different weight percentage.

After a simple thermal treatment in an oxygen atmosphere, a thick, highly protective, bioinert oxide layer develops on the surface of the studied alloys [9,10]. However, to evaluate them as new biomaterials their surface must be carefully characterized, since living tissues will be in direct contact with the most external layers of the implants. Scanning force microscopy (SFM) has become a very valuable tool for understanding the structure and properties of materials surfaces. One of the best advantages of this experimental technique is the possibility of studying the material topography as well as the surface roughness by performing high-resolution imaging.

In the frame of a thorough investigation including elasticity measurements [11], scanning force microscopy has been applied to determine the surface morphology and roughness of these alloys after an oxidation treatment at 750 °C for 24 h [12]. In this work we have broaden this study to a more extended range of oxidation times and we have improved statistics to reduce possible errors coming from inhomogeneities on the surfaces. This allowed us to evaluate the influence of the oxide layer thickness, which is a function of the oxidation time, on the surface roughness.

2. Experimental

Three Ti-based alloys of compositions (in wt%) Ti–7Nb–6Al (T1), Ti–13Nb–13Zr (T2) and Ti–15Zr–4Nb (T3) were investigated in their as-received state, i.e., with a thin native oxide layer, and after an oxidation treatment at 750 °C in air during 1.5 h, 6 h, and 24 h, respectively. This temperature is well below the α–β-phase transition, which takes place at 883 °C [6].

Prior to the oxidation treatment, samples were abraded and polished using diamond pastes with subsequently finer particle size. Colloidal silica was used in the last step to ensure a surface free of mechanical deformation. After polishing, each sample was immersed and cleaned during 10 min in an acetone ultrasonic bath to ensure grease-free and dust-free surfaces prior to measurements.

The surface morphology was analysed by SFM as a function of oxidation time and alloy composition. A commercial instrument (Explorer, Topometrix) was used in the contact mode of operation. In order to minimize the adhesion between tip and sample and get a better topographic resolution, measurements were performed under liquid (deionised water) within a home-made cell mounted on an x–y positioning system (accuracy 200 nm). Si_3N_4, V-shaped cantilevers with normal spring constants of $k = 0.4$ N/m and $k = 2.1$ N/m (Park Scientific Instruments) were used. The applied force was kept in the nanonewton range through the whole series of topographic measurements. Force versus distance curves were regularly obtained during imaging acquisition to check the tip condition.

Topographic images were systematically recorded at different scales to distinguish morphological details but, in order to obtain accurate values, the surface roughness was calculated only from large lateral size images (50 μm × 50 μm). All topographic figures presented here correspond to raw data images, and their present form, as well as the roughness treatment and surface microstructure analysis, were carried out by computer-aided analysis of the SFM images using the available Nanotec™ [13] processing software.

The surface roughness is commonly characterized by the surface root mean square (*rms*),[1] which gives an average roughness by quantifying the fluctuations in the surface height, $h(\mathbf{r}, t)$. For a surface of lateral size L and mean height $\bar{h}$, the rms at a given oxidation time t, is:

$$\mathrm{rms}(L,t) = \sqrt{\frac{1}{L}\sum_{r=1}^{L}[h(\mathbf{r},t) - \bar{h}(t)]^2} \qquad (1)$$

In order to establish a comparison between the oxidation processes for different alloy compositions, the surface morphology prior to oxidation, i.e. of the as-received alloys, was also monitored by SFM and used as a reference.

3. Results and discussion

Fig. 1 shows SFM images (20 μm × 20 μm) of the three Ti alloys in the as-received condition. As previously determined by SEM [7], the fraction of α and β phases in these alloys is comparable for the Ti–13Nb–13Zr (sample T2), whereas for Ti–7Nb–6Al and Ti–15Zr–4Nb (samples T1 and T3) the α-phase clearly predominates. We believe that regions exhibiting different contrast in the images of this figure might be ascribed to the coexistence of α and β phases in the as-received samples if a selective polishing is assumed.

Fig. 2 shows SFM images of the three alloys after oxidation at 750 °C for three different times: 1.5, 6 and 24 h. The

[1] Unless specified, the values of surface roughness presented correspond to the saturation values of the root mean square roughness (rms), determined from the images with largest surface area.

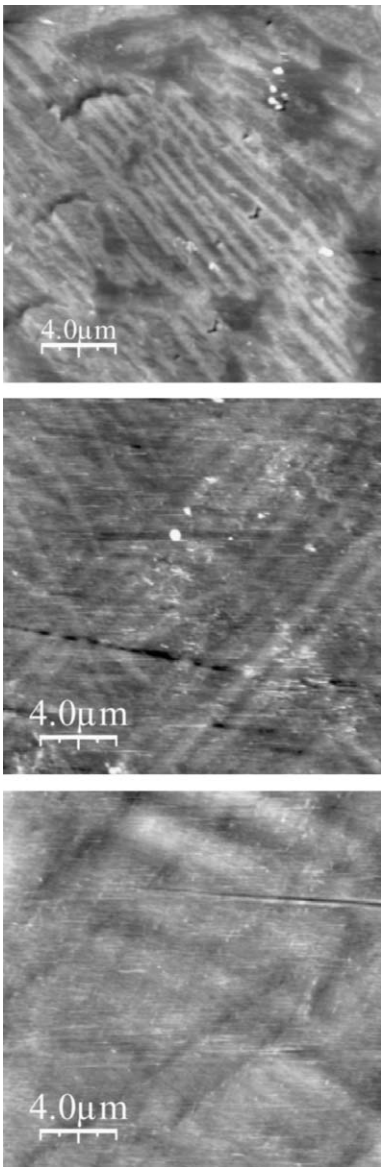

Fig. 1. AFM topographic images of as-received Ti–7Nb–6Al (T1), Ti–13Nb–13Zr (T2), and Ti–15Zr–4Nb (T3) alloys. The total lateral size of the images is 20 μm.

evolution of the topography with oxidation time for each Ti alloy can be clearly seen, being especially noticeable the sudden effect of oxidation for the T3 alloy. For low oxidation times (1.5 h), T1 and T2 present the anisotropic lamellar structure observed for the as-received samples, with a geometric distribution of topographic ridges along well-distinguished directions. At this stage, the surface of the T3 alloy has already developed a characteristic triangular microstructure with a locally quite homogeneous surface but high topographic features at large scale. This polygonal microstructure with a prevailing hexagonal shape is present for the whole range of oxidation times.

The evolution of the surface structure of T1 and T2 alloys is different. After 6 h oxidation, T1 alloy keeps the same overall morphology, while T2 develops a granular structure along randomly oriented lines. Larger oxidation times produce no noticeable microstructural changes in T2, except a smoothening of the observed lines, i.e., the surface evolves to a completely granular structure.

The morphology of samples oxidized for 24 h agrees quite well with SEM images taken on the same samples and reported in a previous work [12]. At this stage, the images show pronounced differences in the topography between the three oxidized alloys, which also differ from that of the as-received materials. The nearly featureless microstructure of T1 contrasts with the mainly granular microstructure of the T2 oxide layer. In both cases a rather regular topography is achieved. Finally, as commented above, the T3 alloy exhibits a polygonal microstructure with a prevailing hexagonal shape. In all cases the morphology leads to well-defined parallel grooves, although they are more pronounced in the T3 case. The different morphology between the three oxide layers can be associated with differences in their chemical composition [10].

Table 1 contains the root mean square (rms) roughness of all samples. To ensure representative and accurate values, they were calculated from 50 μm wide SFM images taken randomly over well-separated regions of the samples. Since they correspond to a statistical analysis through the whole surface, the relatively large error bars give, in fact, an idea of the inhomogeneities of the surface sample morphology. In order to have an overview of these data and to recognize possible trends, they have been represented in Fig. 3. As it can be seen, the as-received samples, with a mirror-like polished surface, show the lowest rms roughness values, just a few nanometers. In particular, the rms value of T3 has been better quoted than in a previous study [12] where smaller area images (10 μm) were used. Since all as-received samples were identically polished, differences in rms are attributed to a selective polishing depending on surface composition. In particular, we note that T1, the only alloy with Al in its composition, presents a slightly larger rms value of 12 ± 3 nm.

For the oxidized samples, the rms exhibits a sharp increase as compared to the as-received values, clearly indicating that the thermal treatment at 750 °C in air gives rise to a solid state reaction which enhances the surface roughness. Additionally, the rms values versus oxidation time have a rather different behaviour for the three Ti alloys. The surface morphology is determined by the oxide layer structure, the oxide growth kinetics and the oxide thickness, which depend on the composition of the base material. As deduced from Table 1 and Fig. 3, T2 and T3 alloys present rms values which can be regarded as constant within the estimated errors for the oxidation time range analysed. These values are, for the final oxidation state, approximately 150 nm for the T2 alloy and 275 nm for T3. This latter value is very close to the rms value of T1 for an oxidation time of 24 h. T2 and T3 have the same alloying elements, so the observed differences in rms could be explained by the different α-phase/β-phase ratio. This is supported by previous results inferred from SEM images of

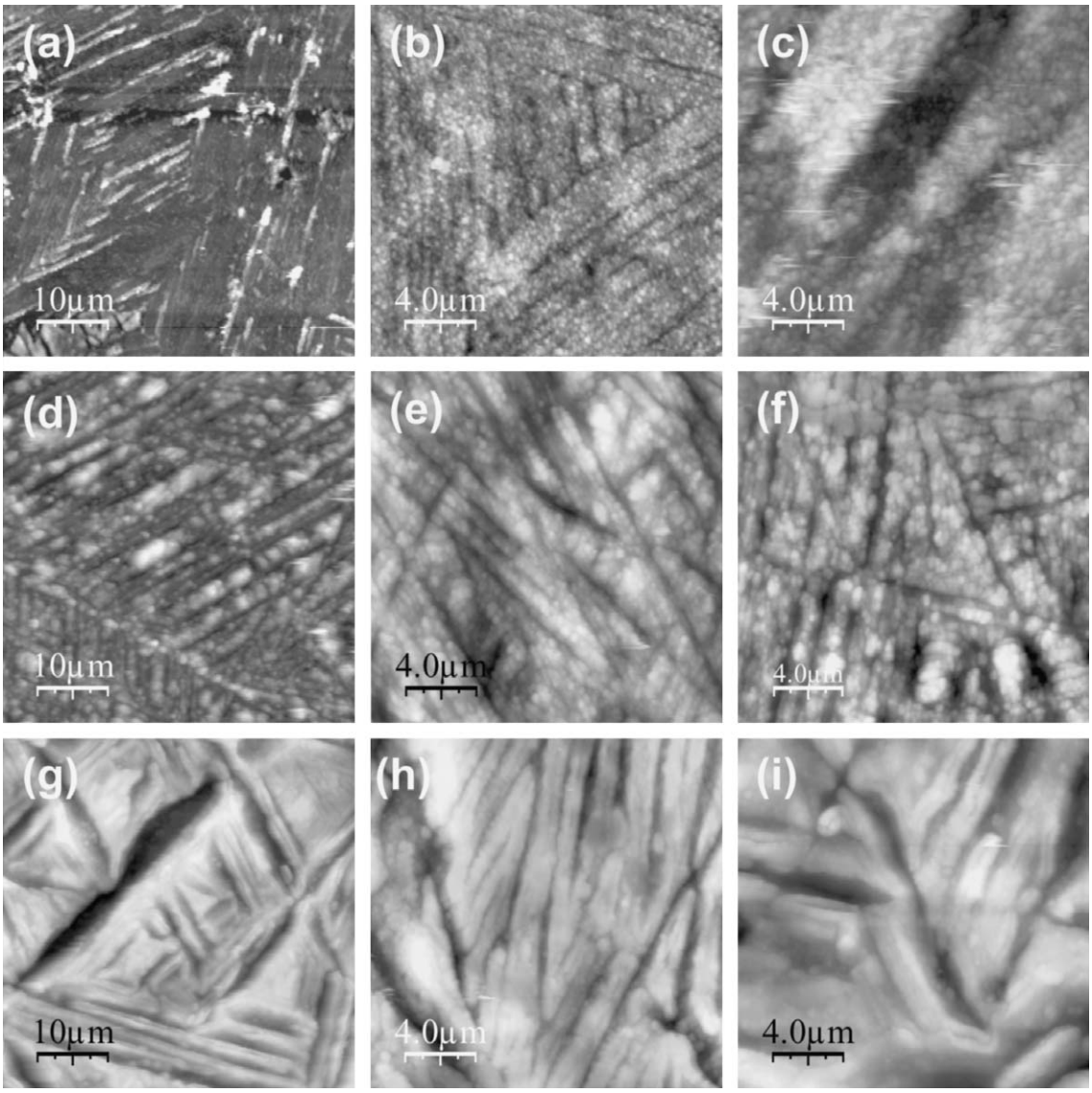

Fig. 2. AFM topographic images of Ti–7Nb–6Al (a,b,c), Ti–13Nb–13Zr (d,e,f) and Ti–15Zr–4Nb (g,h,i) after an oxidation treatment at 750 °C for three different times: 1.5 h (a,d,g), 6 h (b,e,h) and 24 h (c,f,i). To illustrate the overall aspect of the surfaces as well as morphologic details images of two different lateral sizes are presented, 50 μm for (a,d,g) and 20 μm for the rest.

Table 1
Root mean square (rms) roughness values (nm) for the three Ti alloys as-received and after three oxidation processes performed at 750 °C for 1.5, 6 and 24 h

	As-received	Oxidized—1.5 h	Oxidized—6 h	Oxidized—24 h
Ti–7Nb–6Al	12 ± 3	40 ± 10	75 ± 15	240 ± 40
Ti–13Nb–13Zr	3 ± 0.5	125 ± 25	175 ± 25	110 ± 15
Ti–15Zr–4Nb	4 ± 1	275 ± 25	260 ± 40	275 ± 50

the as-received samples [7] that concluded that this ratio is different in both alloys.

As it can be seen in Fig. 3, the T1 roughness increases linearly with oxidation time and only after 24 h it reaches a value rather similar to that of T3. As T1 and T3 alloys have a similar α-phase/β-phase ratio [7], the kinetics of the oxide layer growth has to be considered to explain differences in the roughness for lower oxidation times. Surface roughness develops as the oxide layer thickness does [14]. Since the oxidation reaction takes place at the oxide–metal interface, and the oxidation kinetics is governed by inward oxygen diffusion, the rms is expected to reach a constant value once a critical oxide layer thickness is developed. In fact, the most striking difference between the alloys is the oxide layer thickness for a given oxidation time: after 24 h oxidation, this layer reached a value of around 2 μm for T1, 10 μm

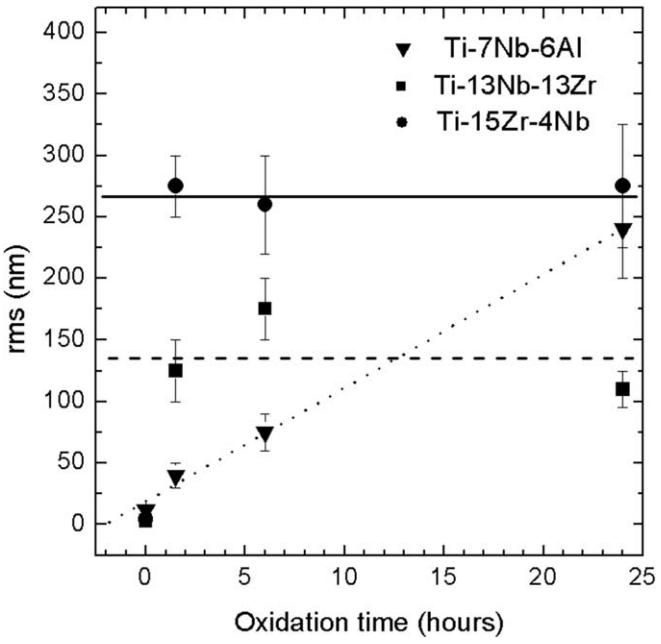

Fig. 3. Evolution of the root mean square roughness values of Ti–7Nb–6Al, Ti–13Nb–13Zr and Ti–15Zr–4Nb alloys as-received and versus oxidation time. The different lines serve as a guide to the eyes.

for T2 and 25 μm for T3, as determined by SEM cross-sectional observations on all three samples [9]. According to previous XAS (X-ray absorption), XPS (X-ray photoelectron spectroscopy), RBS (Rutherford backscattering spectroscopy) and ERD (elastic recoil detection) studies [10,15], oxidized T1 sample surface is rich in Al_2O_3, whereas the oxide layer of T2 and T3 samples is mainly composed of TiO_2. The extremely good oxidation resistance of Al_2O_3 can help to explain the much slower oxidation kinetics of sample T1. Indeed, according to SEM and supported by Fig. 3, alloys T2 and T3 have already reached a thickness of approximately 2 μm after 1.5 h oxidation, a similar value to the thickness of the T1 sample at 24 h. This suggests that there is a critical oxide layer thickness from which rms roughness has a more or less constant value, and this critical value is around 2 μm. For thicknesses above this value, the rms values remain approximately constant: 240 nm for T1, 150 nm for T2, and 275 nm for T3. There seems to be a correlation between these final rms values and the α-phase/β-phase ratio present in the alloys. This ratio is similar for T1 and T3 samples, which also have similar rms values, whereas for T2 the ratio is lower, being the final rms value lower in this case.

4. Conclusions

SFM investigations were performed to characterize the surface morphology and topography of the alloys Ti–7Nb–6Al, Ti–13Nb–13Zr and Ti–15Zr–4Nb, which were studied in the as-received state and after a thermal treatment in air at 750 °C for different times. The purpose of this oxidation process is to generate an oxide surface layer on the material with improved wear and corrosion resistance and higher roughness, which would provide higher adhesion between tissue cells and implant surface. According to the SFM results, the thermal treatment leads to a surface roughness increase as the thickness of the oxide scale grows, up to a final roughness value, which is achieved after the oxide layer reaches a critical thickness of about 2 μm. This final value strongly depends on the α-phase/β-phase ratio of the base alloys.

Acknowledgments

The authors are gratefully acknowledged to Prof. G. Fommeyer from Max Planck Institut für Eisenforschung (Düsseldorf) for kindly supplying the Ti alloys specimens. This work has been supported by Project MAT-2004-00150 of the Spanish MEC and Projects 07N-0050-1999 and 07N-0066-2002 of the Spanish "Programa de Tecnología de los Materiales de la Comunidad Autónoma de Madrid". A.G. and C.O. thank the Spanish MEC for financial support through the "Ramón y Cajal" and the "Formation and Mobility" (ref. PR2004-0425) Programmes. C. Munuera thanks the Spanish MEC for a pre-doctoral scholarship.

References

[1] H.J. Breme, V. Biehl, J.A. Helsen, in: J.A. Helsen, H.J. Breme (Eds.), Metals as Biomaterials, John Wiley & Sons, Chichester, 1998 (Chap. 2).
[2] D.H. Kohn, P. Ducheyne, in: D.F. Williams (Ed.), Medical and Dental Materials, Serie Materials Science and Technology, vol. 14, VCH, Weinheim, 1992 (Chap. 2).
[3] S.G. Steinemann, in: G.D. Winter, J.L. Leray, K. De Groot (Eds.), Evaluation of Biomaterials, Wiley, New York, 1980.
[4] Y. Okazaki, S. Rao, Y. Ito, T. Tateishi, Biomaterials 19 (1998) 1197.
[5] M.A. Khan, R.L. Williams, D.F. Williams, Biomaterials 20 (1999) 765.
[6] H.L. Freese, M.G. Volas, J.R. Wood, in: D.M. Brunette, P. Tengvall, M. Textor, P. Thomsen (Eds.), Titanium in Medicine, Springer-Verlag, Berlin, 2001, p. 25 (Chap. 3).
[7] M.F. López, A. Gutiérrez, J.A. Jiménez, Electrochim. Acta 47 (2002) 1359.
[8] M.F. López, A. Gutiérrez, J.A. Jiménez, Surf. Sci. 482 (2001) 300.
[9] M.F. López, J.A. Jiménez, A. Gutiérrez, Electrochim. Acta 48 (2003) 1395.
[10] M.F. López, L. Soriano, F.J. Palomares, M. Sánchez-Agudo, G.G. Fuentes, A. Gutiérrez, J.A. Jiménez, Surf. Interface Anal. 33 (2002) 570.
[11] Carmen Munuera, Thomas Reinhold Matzelle, Norbert Kruse, María Francisca López, Alejandro Gutiérrez, José Antonio Jiménez, Carmen Ocal, in preparation.
[12] C. Morant, M.F. López, A. Gutiérrez, J.A. Jiménez, Appl. Surf. Sci 220 (2003) 79.
[13] Nanotec Electronica, E-28760 Tres Cantos. Available from: <www.nanotec.es>.
[14] C. Munuera, J. Zúñiga-Pérez, J.F. Rommeluere, V. Sallet, R. Triboulet, F. Soria, V. Muñoz-Sanjosé, C. Ocal, J. Cryst. Growth 264 (2004) 70;
P. Klapetek, I. Ohlídal, K. Navrátil, Microchim. Acta 147 (2004) 175.
[15] A. Gutiérrez, M.F. López, J.A. Jiménez, C. Morant, F. Paszti, A. Climent, Surf. Interface Anal. 36 (2004) 977.